Journal of Advanced Research in Applied Sciences and Engineering Technology

Journal homepage:
https://semarakilmu.com.my/journals/index.php/applied_sciences_eng_tech/index
ISSN: 2462-1943

TLBO trained an ANN-based DG integrated Shunt Active Power Filter to Improve Power Quality

Venkata Anjani Kumar Gaddam[1,*], Manubolu Damodar Reddy[1]

[1] Department of Electrical and Electronics Engineering, S.V.University College of Engineering, S.V.University , Tirupathi-517502 Andhra Pradesh, India

ARTICLE INFO

Article history:
Received 20 October 2023
Received in revised form 26 November 2023
Accepted 1 March 2024
Available online 17 April 2024

Keywords:
Biogeography-based optimisation (BBO), solar cell , Teaching learning-based optimization (TLBO), Power Quality, Total Harmonic Distortion, Shunt Active Power Filter, ANN-Controller Tuning, PI-Controller Tuning

ABSTRACT

In terms of power quality, the rising number of nonlinear loads in modern use has caused warning signs for power systems and power engineering professionals. Every day, utilities have to deal with harmonic distortion caused by a growing number of non-linear power electronic equipment. To keep the system's power supply in good condition, a shunt active filter is used to filter out unwanted harmonics in the signal. This study presents a practical and low-cost method for reducing harmonics and enhancing distribution network power quality by means of the use of PV-integrated Shunt Active Power Filters (SAPF). With a teaching-learning-based optimized artificial neural network controller (TLBO-ANN) the required DC power is extracted from the PV module. SAPF's TLBO-ANN algorithms are intended to increase system performance by reducing total harmonic distortion (THD). Here, the research work was performed in three stages to mitigate grid current harmonics. The first-stage SAPF system comprises a three-prong voltage source converter and uses DC power derived from photovoltaic panels. The P&O algorithm is used to get the maximum power out of a photovoltaic array. In the second stage, the BBO algorithm is used to fine-tune a conventional PI controller, resulting in values optimal gain values that increase the controller's performance. Furthermore, it is intended to use the BBO-PI controller's input and output values as training data for the ANN controller. This ANN controller is currently being tuned with the TLBO algorithm to find optimal values for the weight and bias parameters. In the third stage, the converter in PV-SAPF will inject the active power required by the load by using active current control theory, which means the inverter of SAPF is working like DG as well as the active power filter. Employing MATLAB simulations, we concluded that the proposed method is extremely adaptable and highly efficient in lowering harmonic currents that are brought on by non-linear loads.

1. Introduction

For a long time, fossil fuels seemed to be the primary source of energy. However, they have several drawbacks, including limited availability, exhaustibility, and non-recyclability. Pollution from them contributes to wider problems, like a warming planet. As a result, there is a movement around

[*] *Corresponding author.*
E-mail address: anjishelectrical@gmail.com

https://doi.org/10.37934/araset.43.2.93110

the world to introduce the next generation to more eco-friendly technologies. [1-3] As PV-based systems continue to improve and gain popularity as an alternative to traditional energy sources, their use in a broad range of environments is only going to grow. The introduction of harmonics into the system is a direct result of the widespread use of power electronics devices and nonlinear loads. Most electrical devices will function normally with total harmonics below 5%, as specified by IEEE standard 512-2014 [4]. There has been a lot of dependence on passive filters to mitigate harmonics, although they have several drawbacks. When the number of unwanted harmonics rises, it consequently increases the complexity of the network's design and the possible occurrence of a resonance problem. As it can filter harmonics from the PV module's converted DC output, APF that is powered by PV is growing in popularity. The initial investment in a photovoltaic system is substantial, so getting the most energy out of it is a no-brainer. It is combined with a Maximum Power Point Tracking (MPPT) algorithm for optimizing PV system performance. MPPT modeling of PV systems is reported in [5]. Several factors, including irradiance level, temperature, and the configuration of the PV system, affect the quality of power obtained from the PV-APF in a system that exists in the real world.

Inadequate power factor, reactive power compensation, and high current harmonics might all be solvable with the help of a shunt active power filter (SAPF) [6]. See Figure 1 (on the next page) for a visual representation of the PV-SAPF setup, which consists of the DC voltage supplied by the PV panel, the active filter controller, and the voltage source converter (VSI). Based on the control signal from the control unit, the gates of the VSI operate like that to achieve the need for compensating current to the PCC to provide reactive power to the load [7]. Reactive power control for the grid is provided by the DC-link capacitor of the VSI, which is fed by a PV source and located on its input side [8]. The DC component cannot be connected directly to the three-phase power grid without a VSI [9].

The VSI switching operation can be analyzed with either reference-generating methods or control techniques. After extracting compensating signals from affected signals employing reference current generation concepts, The SAPF switching devices can be controlled with the help of various references current generation methods [10] to implement the SAPF control techniques. Several authors have compared various SAPF management approaches [11,12].

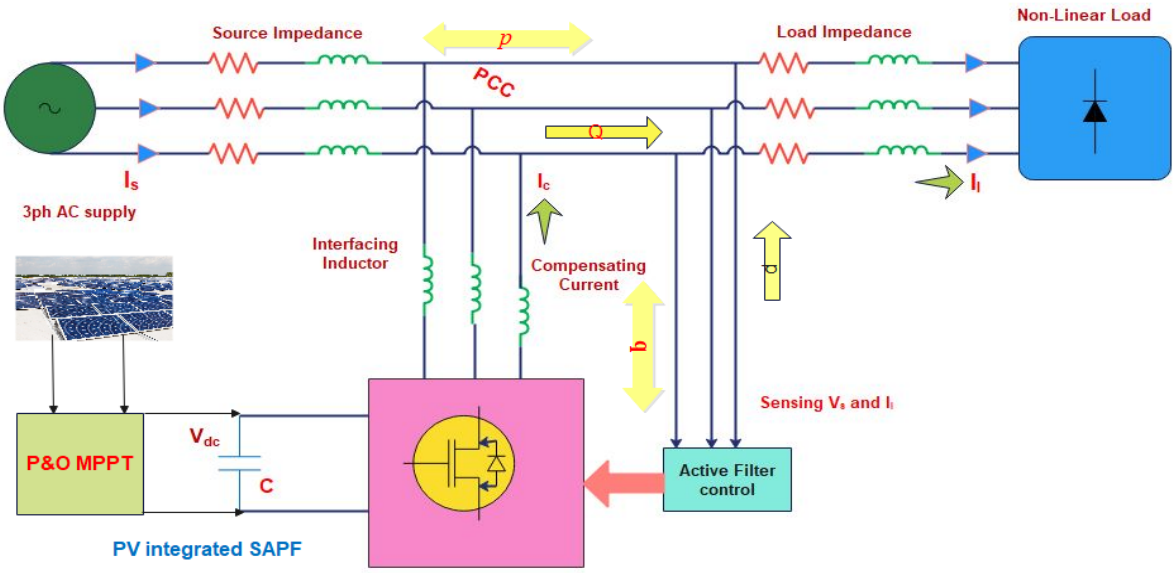

Fig. 1. PV integrated SAPF in a distribution system

The PI-controller, an integral component of reference current theory, is designated to mitigate harmonics. It is essential to fine-tune the PI controller's values for optimum performance. The conventional approach to tuning the PI-controller gains relies on linear modeling, which typically yields inadequate settings for the gains [13,14]. To this end, many different met heuristic optimization strategies are used in PI-controller tuning. To reduce current harmonics and open up new possibilities for the converter [15], several different control methods exist. Example algorithms include the Atom Search Optimisation (ASO) [16–20], the Genetic Algorithm (GA) [21], and the Simulated Annealing (SA).

An ANN is a network designed and programmed to perform similar tasks as the human brain. The brain consists of billions of interconnected cells called neurons. The strength and organization of connections between interneuron determine the overall network's behavior. Adjustments are made to the weights during network training [22]. So the Artificial Neural Network (ANN) techniques provide the most effective method for controlling the DC voltage of SAPF[23,24] through the training of weights and biases. Several approaches can be used to learn weights [25]. Methods like the Steepest Descent approach to learning variables, the Levenberg-Marquardt method, and the Widrow-Hoff (W-H) method are just a few examples.

The principles of Active current control theory are applied in this study. To generate the required gating pulses, a hysteresis current controller [26] uses an estimation of reference currents. The ANN controller's performance for a DC-link voltage can be improved through careful adjustment of the weight and bias values. The weight and bias of the ANN controller are optimized using a teaching and learning-based optimization algorithm.

2. Concept PV Cell

This silicon-based semiconductor operates as a PN junction [27,28]. It's the fundamental component of any photovoltaic setup. Light excites electrons and holes when it strikes a semiconductor's surface. As a result, an electric field is generated due to the presence of positive and negative terminals. As shown in Figure 2, when light strikes the surface of a semiconductor, electrons and holes are created. The P-region bubbles stand in for the presence of holes, while the N-region bubbles denote the presence of electrons. As shown in the middle of Figure 2, positive and negative terminals are thus formed. Electrons flow towards P-type semiconductors and holes towards N-type semiconductors when both terminals are in contact with a conductor. The plus and minus signs at either end of this diagram denote P-type and N-type semiconductors, respectively. This causes electricity to flow between them in the form of a current. With a PV system, solar energy can be transformed into electricity immediately. For a solar power generation system to generate a significant amount of electricity, a large number of PV cells must be connected in series or in parallel to create a solar module, solar panel, or solar array, as shown in Figure 3.

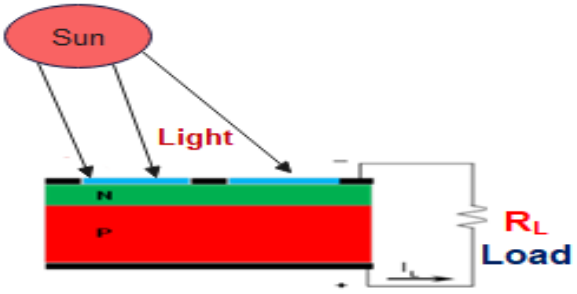

Fig. 2. Basic structure of Photovoltaic system

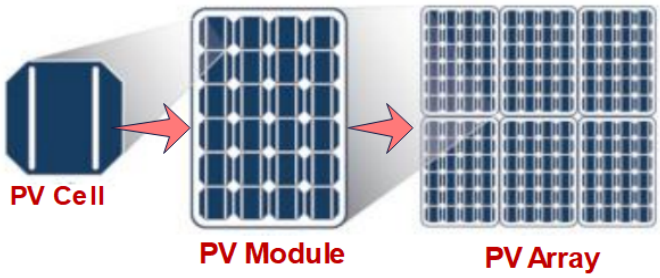

Fig. 3. Connecting diagram of solar cell, module, array

3. PV System Modeling

In Figure 4, we see the circuit for the PV cell, which uses a single diode and is wired in parallel with the mains. Resistance in series is denoted by R_s, and resistance in shunt is denoted by R_{sh}. The cell operates in two settings, and its power consumption is proportional to the amount of sunlight it receives [29]. One is the current in a closed circuit, and the other is the potential difference between the terminals in an open circuit.

When the diode is open, there is no voltage across it, and the current through the short circuit is equal to the current through the current source, Voc.

The equation gives information about PV's properties.

$$I = I_L - I_0 \left(e^{(v+R_s/n_s v_t Q_d)} - 1\right) - \frac{v+R_s}{R_{sh}} \quad (1)$$

In this Eq. (1), V represents the array voltage, I represents the array current, I_L represents the light current, I_0 represents the reverse saturation current of the diode, Q_d represents the diode's ideality factor, n_s represents the number of series cells, R_s represents the series resistance,R_{sh}represents the shunt resistance, V represents the thermal voltage, and I_d represents the diode current.

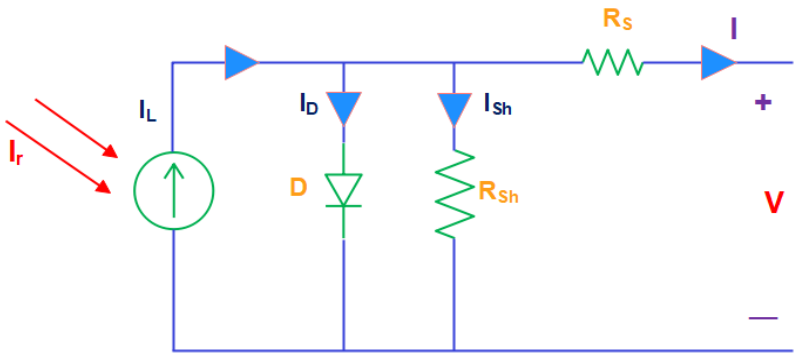

Fig. 4. Single line diagram of photovoltaic system

Table 1 details the parameters and technical specifications of the Sun Power SPR-315E-WHT-D modules used in this analysis.

Table 1
PV panel specifications

Parallel Strings	12
Series –Connected Modules per String	7
PV Module Name	Sun power SPR-315E-WHT-D
Max power	315.072
Open –circuit voltage(V)	64.6
Short –circuit current(A)	6.14
Voltage at MPPT (v)	54.7
Current at MPPT (a)	5.76
Irradiation (w/m^2)	1000

4. Perturb and Observe (P&O) MPPT

Since the P&O MPPT algorithm is the most practical MPPT algorithm in terms of implementation and incorporation in commercial charge controllers, it is given extra attention in this work. Like many other derivatives, the P&O experiences the aforementioned trade-off between dynamic response (speed) and steady-state oscillations (discussed in the introduction). In other words, there was a trade-off between responsiveness to changes in the environment and speed. To find out how well the MPPT algorithm works, we will look at its tracking time (dynamic response), steady-state oscillations, and efficiency. In this paper, we use these three factors as the basis for assessing MPPT's performance. The tracking time constitutes an essential performance evaluation parameter for the MPPT algorithm, as defined according to [30], as the time taken by an MPPT algorithm to reach 95% within the maximum average power at MPP.

Figure 5 is a flowchart depicting the P&O algorithm [31,32]. The algorithm constantly monitors the current and voltage of each PV module and, by extension, the power output. Power readings are compared to readings taken at the same time as a prior instant. As shown in the diagram, a linear perturbation shifts the operating point towards or away from the maximum power point, depending on the sign of the change. The size of the perturbation δD used in the flowchart directly affects the P&O's performance. At steady state, larger values of δD result in larger oscillations, while smaller values of δD result in smaller oscillations and a slower dynamic response.

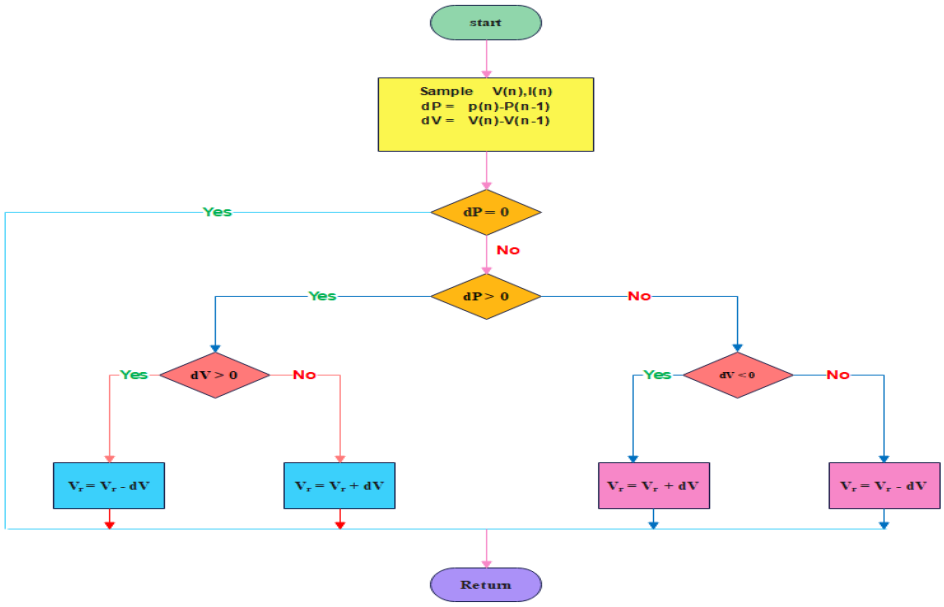

Fig. 5. Flow chart representation of P&O MPPT

5. Artificial Neural Network (ANN)

Considering that neural networks form the backbone of the human brain's architecture, the term "Artificial Neural Network" has been obtained from the field of neuroscience. Just like the human brain, artificial neural networks have many layers of neurons that connect to other layers in complex ways. Nodes are the names given to these nerve cells in Figure 6. Typically, a nominal neuron will have one or more outputs and n inputs (x_1, x_2,⋯, x_j, x_n) where x_1, $x_2$and x_j, x_n the individual contributions and outputs of neurons. We can see the connection between these two in Figure 5. Yi [33] represents the value produced by the neuron, which is formed by first adding up all of its inputs and then passing that total through the activation function.

$$Y_i = f_i\left(\sum_{j=1}^{n} w_{ij} * x_j + b_i\right) \quad (2)$$

where w_{ij} = This is the synaptic weight of the link between the initial input neuron and the final output neuron.

b_i = The i[th] neuron bias,
x_j = The input representation of j[th] neuron
F = An activation function that regulates network behavior.

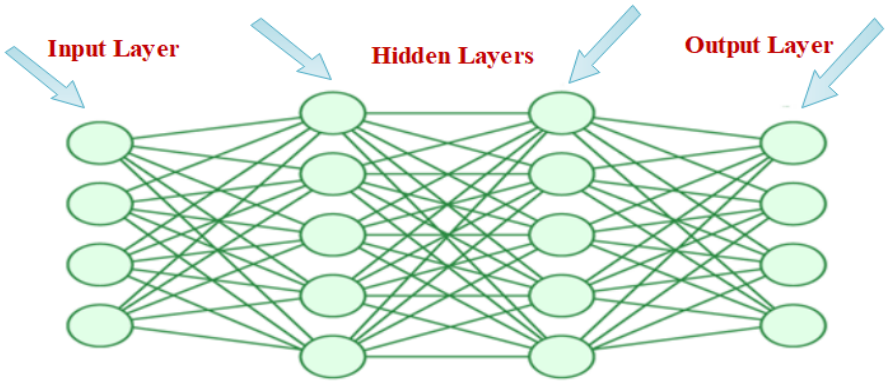

Fig. 6. ANN architectural design

Neural networks adapt to input data by modifying the weights of connections, which may include biases, as well as occasionally adjusting the number of layers and neurons.

6. An Overview of the TLBO Algorithm

One of the recently proposed population-based algorithms is called teaching-learning-based optimization, or TLBO for short. The TLBO technique, developed by Rao *et al.,* in 2011, was presented in the paper [34]. It was conceived as a response to the phenomenon of classroom instruction and learning [35]. For purposes of the TLBO population-based learning algorithm, the entire class is considered a population, with each student treated as a discrete member of the population. In order to achieve this goal, it is anticipated that the class will have gained knowledge by the lesson's conclusion. The process can be broken down into two distinct phases: the "teacher phase" and the "learner phase," respectively. This is the basis for reaching this goal.

a. Teacher phase

The best student in the class with the best solution becomes the instructor. When it comes to a given topic, the teacher is held in the highest regard because of the widespread belief that they know more than anyone else. As a result, other students benefit from the instructor's knowledge and experience. If a student offers a better solution than the teacher, the student will take over the teacher's responsibilities. In the kth iteration, the ith learner's knowledge is revised using the equation 3.

$$X_i^{new} = X_i + r_I(X_T - T_F{}^i . X_{mean}) \quad (3)$$

The teaching factor, $T_F{}^i$ can be calculated from the above scenario using the following equation 4: where "X_T," is the teacher's knowledge, "r_I ′′ is a two-digit random number between 0 and 1, "X_{mean}," is the students' average achievement, and "r_I ′′ is a random number between 0 and 1

$$T_F{}^i = round\ [1 + rannd(0,1)] \quad (4)$$

When the teacher phase is complete, the students' knowledge has been brought up to date, and the resulting values can be used as inputs in the subsequent learner phase.

b. Learner phase

Students learn more by talking to each other in a real classroom. The TLBO learner phase is based on this. This step compares the **ith** student's knowledge to a randomly selected **jth** student (equation 5). Students learn more by talking to each other in a real classroom. The TLBO learner phase is based on this. This step compares the **ith** student's knowledge to a randomly selected **jth** student (equation 6).

If $f(X_i) < f(X_j) \quad then, \quad X_i^{new} = X_i + r_I(X_i - X_j)$ (5)

If $f(X_i) > f(X_j) \quad then, \quad X_i^{new} = X_i + r_I(X_j - X_i)$ (6)

As shown in Equation 7, if the **jth** student finishes the learning phase with more knowledge, the **ith** student can benefit.

If $f(X_i^{new}) < f(X_i)\ than,\ X_i = X_i^{new}$ (7)

The two-part TLBO algorithm (teacher phase, learner phase) will run until either the termination condition is met or the maximum number of iterations is reached.

7. Proposed Methods

7.1 Tuning Of PI Controller By Using BBO Algorithm

The PI controller maintains DC link voltage stability, which is critical to the performance of a PV-integrated SAPF. The critical controller's PI controller has a complex mathematical process for determining the gain (K_P, KI) values. The PI controller's calculated gains are suboptimal. In this work, biogeography-based optimization (BBO) is used to calculate the optimal gains for the PI controller.

Integral absolute error (IAE), represented in Figure 7 as the difference between actual and desired DC voltages, is the objective function. The BBO algorithm optimizes the PI controller's gains by optimizing these objective functions.

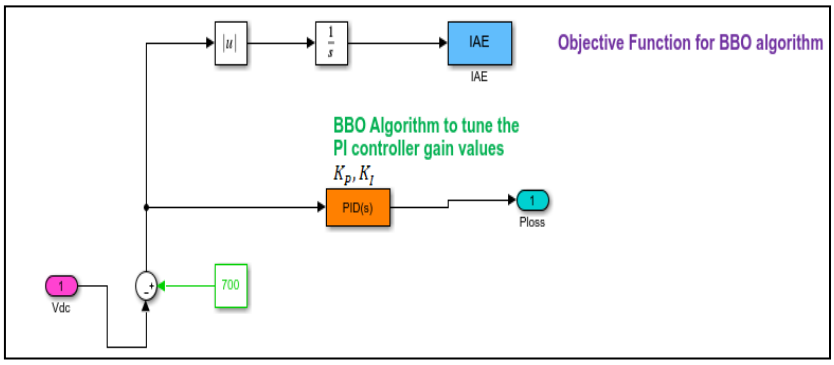

Fig. 7. Simulink model of PI controller tuning with BBO algorithm

7.2 TLBO trained ANN Controller

The main objective of a neural network algorithm is to obtain appropriate weights and biases for the network to be as accurate as possible. Multiple techniques are used to determine the optimal values for an ANN's weights and biases. In this study, we used a method called TLBO. Figure 8 shows that the inputs (e) and outputs (out) of the BBO-PI controller are used as a source of data for the neural network controller.

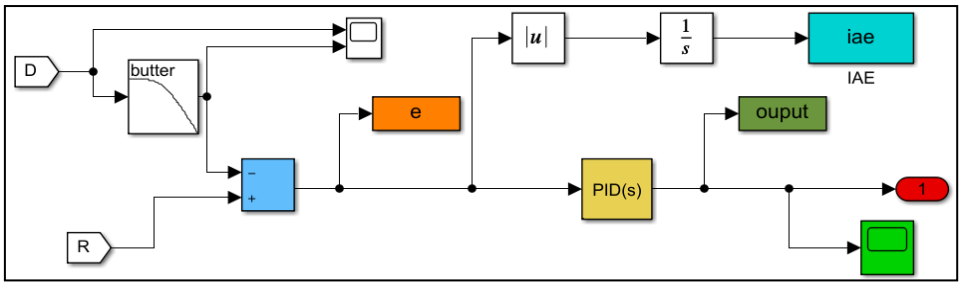

Fig. 8. Output (o) and input (e) representation in the workspace for the BBO-PI controller

The following code sets up the neural network. After obtaining the BBO-PI controller's input and output values, the hidden neurons can be initialized to complete the ANN's configuration. The network's weights and biases are then extracted. Next, a pre-trained neural network's weights and bias are defined using the TLBO algorithm, with the root mean square error serving as the objective function in this case.

Step-by-step approach for TLBO-trained ANN
Step 1: Get the input (e) from the BB0-PI controller's workspace.
Step 2: Get the target (output) from the BBO-PI controller's workspace.
Step 3: Provide the Hidden Neurons
Step 4: Use hidden neurons to set up the Feed Forward Neural Network.
Step 5: Give the neural network the input and output values that were given.
Step 6: Make the initial weights and biases.

Step 7: Use the root-mean-square error as the goal function and use the inputs, target values, and parameters (i.e., weights and bias) of a feed-forward ANN.
Step 8: The TLBO algorithm is used to train the neural network, which gives us the new weights, biases, and errors.
Step 9: Set up the Feed Forward Neural Network again with the new weights and biases.
Step 10: Do steps 7 through 9 again and again until the objective function is very low.

The network has converged when the mean square error (NMSE) decreases to an acceptable level while the synaptic coefficients are optimized to a final value. It is also possible to interrupt the learning process by reducing the number of iterations. A flowchart of the training algorithm is shown in Figure 8. The BBO-PI controller will ultimately replace the feed-forward neural network depicted in Figure 9 for a given input and output.

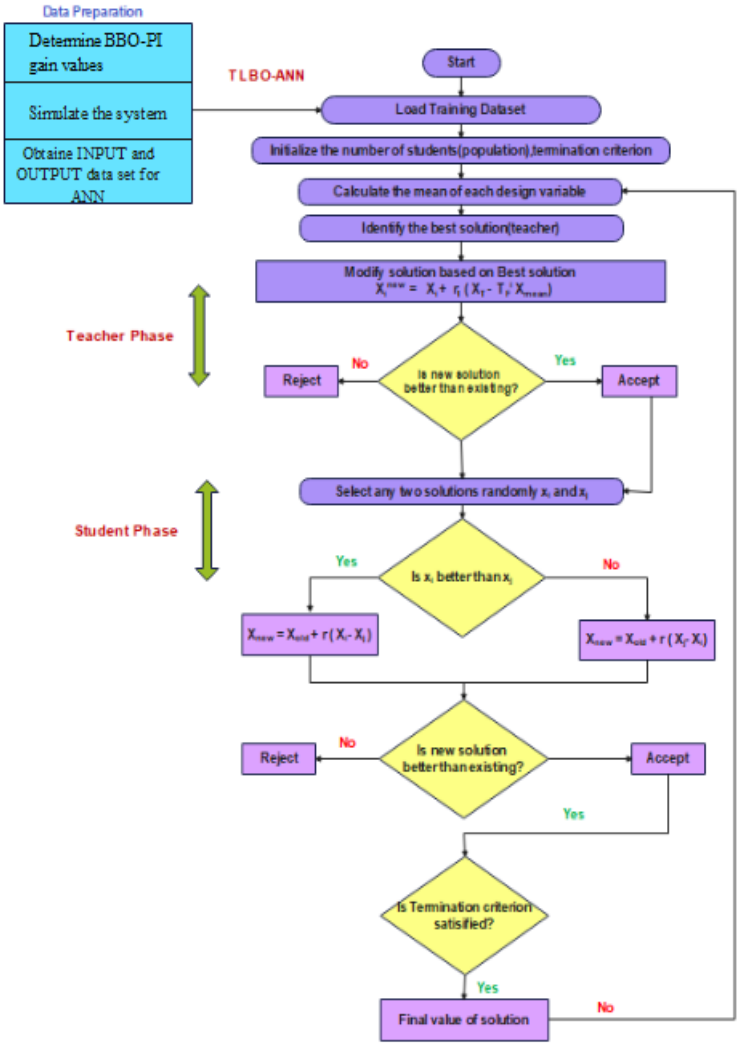

Fig. 9. Flow chart representation of TLBO-ANN

With a certain input and output, we will finally get the feed-forward neural network block and inside layering structure shown in Figure 10. The PSO-PI controller will replace this feed-forward neural network block.

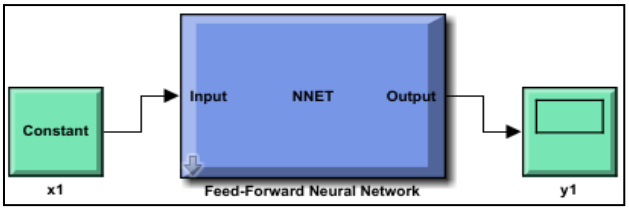

Fig. 10. Simulink block obtained from TLBO-ANN algorithm

7.3 Active Current Coefficient Control

With this theory, we can determine the precise amount of active current that the PV system must supply to the load. First, the phase-to-phase grid voltage is sensed and transformed into the phase-to-ground voltage; next, this voltage is transformed into the a-β reference frame voltage via the Clark transformation; finally, the inverse Clark transformation is used to convert the a-β frame voltage back into the a-b-c frame voltage. From there, we can derive a-b-c grid voltages (Vg_a, Vgb, and Vg_c). A band-pass filter is applied to these voltages to remove higher-order harmonics, and here we create some exclusive vectors for PV grid synchronization. Again, measuring the load current is essential. Find the active current coefficients for lines a, b, and c using the given load currents and the unique vectors, as shown in Figure 11. Finally, we'll take an average of these values to determine the actual active current needed by the load (I_L).

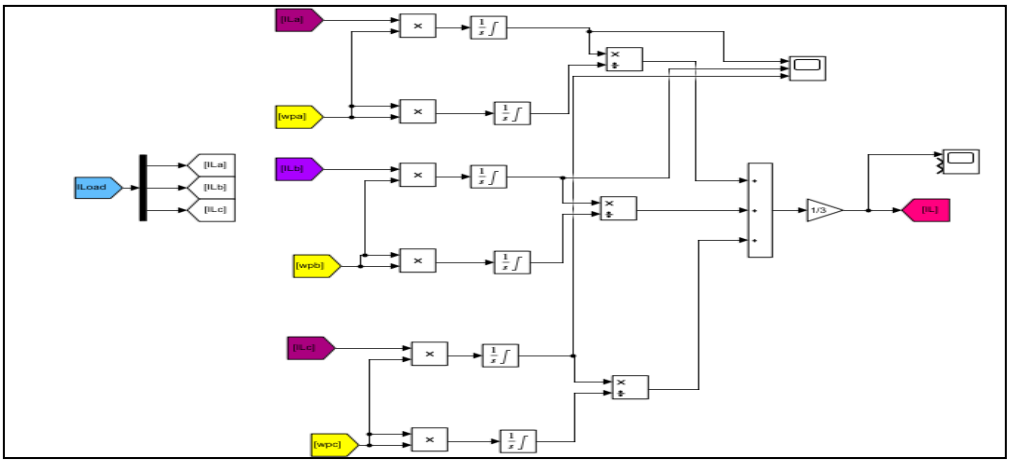

Fig. 11. Simulink representation of Active Current Coefficient theory

8. Results and Discussion

The simulated system includes a shunt active filter run on solar photovoltaic's (PV) to reduce harmful harmonics and enhance power quality. To generate gate pulses for the inverter, a voltage-source inverter (VSI) incorporates a hysteresis controller. Maximum Power Point Tracking (MPPT), a technique based on P&O, is used in the model to get the maximum power from the solar panel. SAHF was included and excluded from the model in the evaluation of the network. The V-I traits can be determined through statistical examination. To reduce current harmonics and promote power enhancement, a photovoltaic (PV)-based shunt active filter was tested and analyzed in MATLAB/Simulink. The photovoltaic panels received solar irradiation at 1000 w/m2 and 250 °C as their input. The short-circuit current, open-circuit voltage, and maximum power output are shown in Figure 12.

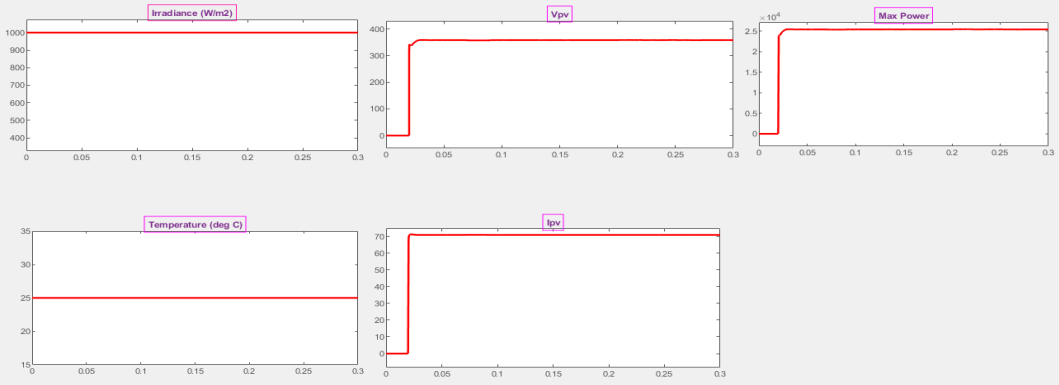

Fig. 12. Output characteristics (P_{max},V_{PV},I_{PV},Irradiation) of PV module

8.1 Harmonic Spectrum of PV-SAPF with conventional PI controller

Here, the PV-integrated SAPF uses a conventional PI controller to regulate the DC capacitor voltage. Figure 13 demonstrates that the THD on the grid can be reduced from 18.2% [36,37] (without SAPF) to 3.08% when using PV-SAPF with a conventional PI-based controller.

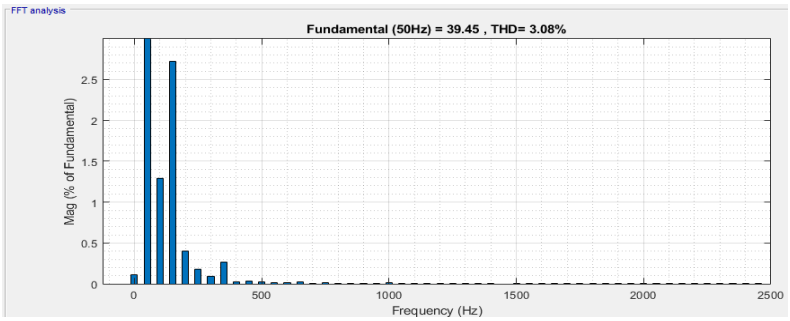

Fig. 13. Source current FFT analysis of PI based PV-SAPF

8.2 Harmonic Spectrum of PV-SAPF with BBO trained PI controller

However, in this case, the PV-integrated SAPF uses a BBO-trained PI controller to control the voltage of the DC capacitor. K_p and K_i gains of the PI controller will be fine-tuned using a biogeography-based optimization (BBO) strategy to optimize the error voltage (IAE), the objective function. If a nonlinear load is connected to the grid at the same time, in order to maintain the sinusoidal shape of the grid current, SAPF is going to inject a compensating current into the PCC. The harmonic spectrum of the PV-SAPF with the BBO-PI controller is shown in Figure 14. The figure clearly displays the THD value at source current to be 0.91%, demonstrating a drop from 1.18% to 0.91%. The BBO-PI controller's settings are listed in Table 2.

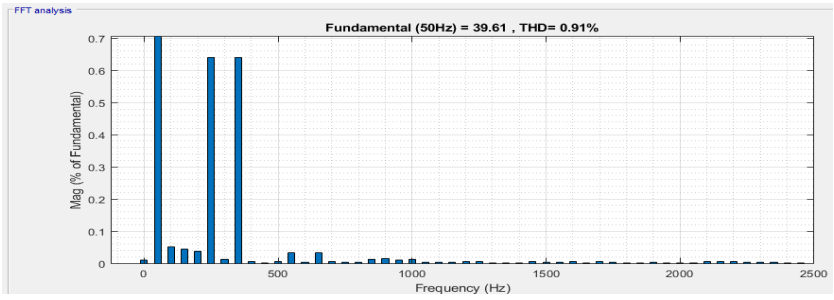

Fig. 14. Source current FFT analysis of BBO trained PI based PV-SAPF

Table 2
BBO Parameters

BBO Parameters	Values
Max number of Iterations	100
Number of Tunable Variables	2
Keep rate	0.2
Total Quantity of Kept Habitats	5
Total Quantity of New Habitats	20
Total Populations	25
Alpha	0.9
Mutation	0.1
Emigration and Immigration rates	1

8.3 TLBO trained ANN based PV integrated SAPF

Here, the TLBO-ANN controller Simulink block has taken the place of the BBO-PI controller. This Simulink block was taken from Figure 10 and is shown interacting with a feed-forward neural network in Figure 15. The source current's total harmonic distortion (THD) appears to have dropped to 0.55%, according to the results.

Figure 16 illustrates the waveforms of the source voltage and source current. The harmonic spectrum of the source current is depicted in Figure 17. The TLBO-ANN controller's converging spectrum can be seen in Figure 18.

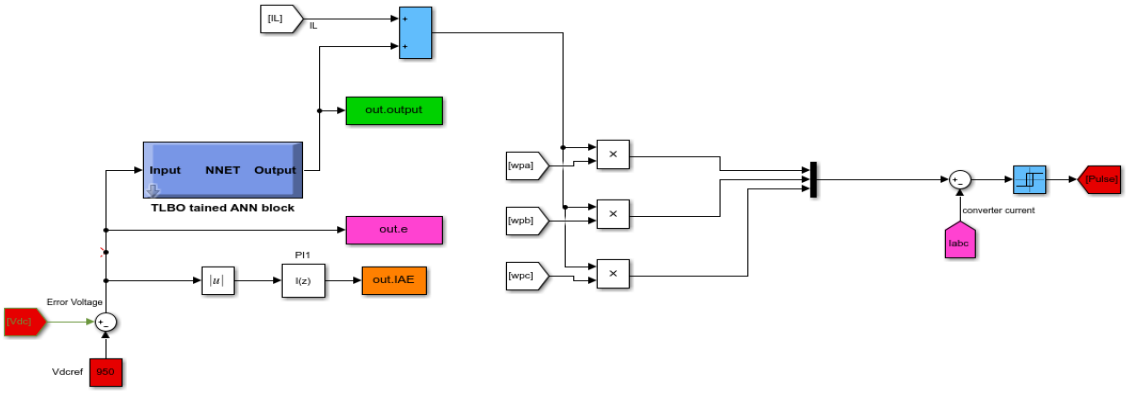

Fig. 15. Controlling the DC voltage in a PV- SAPF with an TLBO-ANN regulator

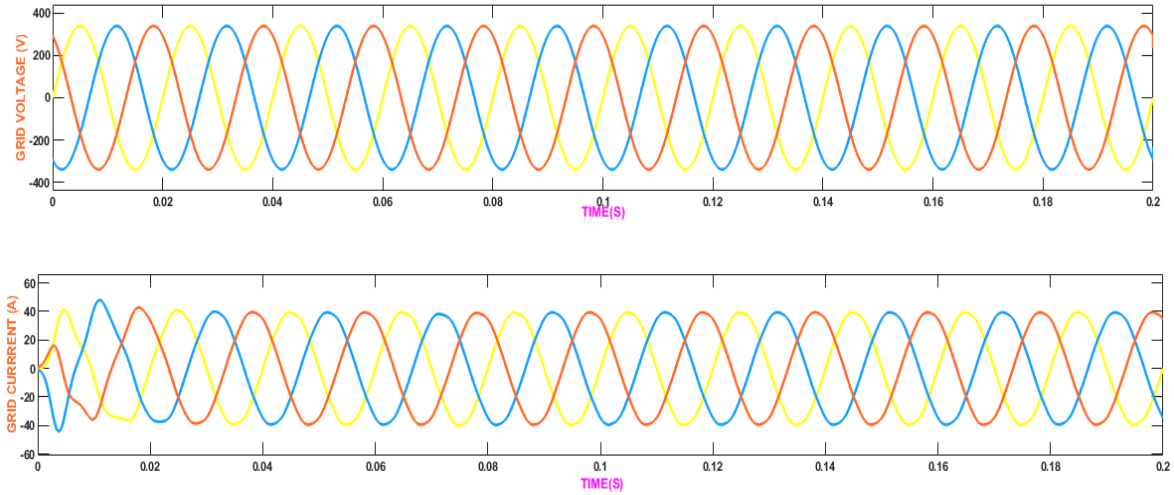

Fig. 16. The waveforms of the V_S,$I_S$by using TLBO trained ANN based PV- SAPF

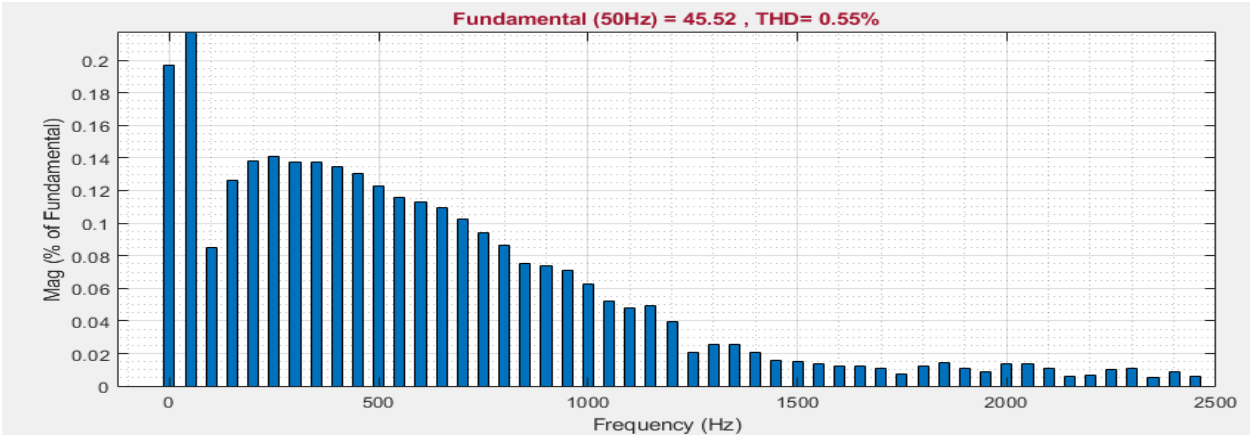

Fig. 17. THD result of I_S (Grid current) by TLBO tuned ANN based PV-SAPF

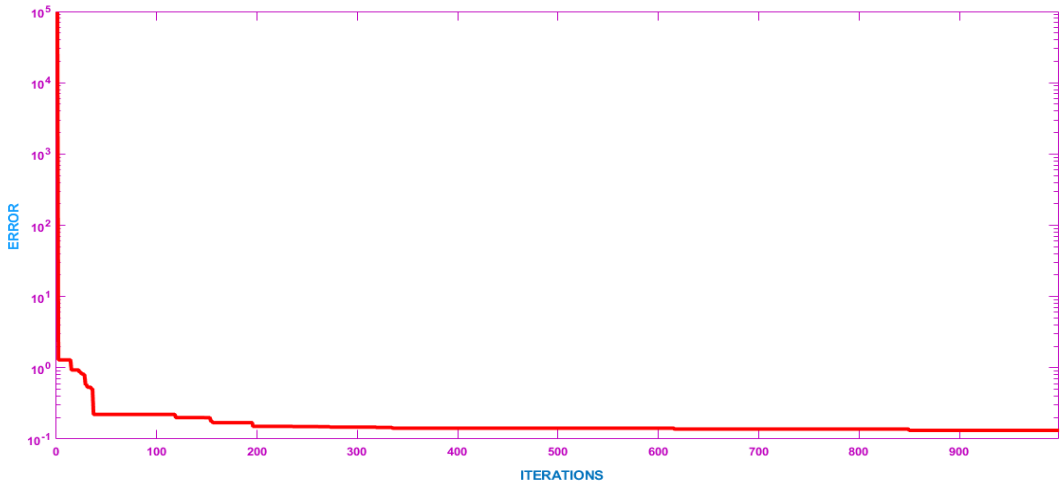

Fig. 18. Converges graph for the TLBO-ANN based PV- SAPF

The parameters for the TLBO-ANN are detailed in Table 3. Table 4 provides an overview of how the SAPF performed in each of the four scenarios.

Table 3
The data to a TLBO-trained ANN

The maximum number of iterations	1000
Quantity of Students	50
Teaching Factor	1
Hidden Neurons	12
Total number of Variables	1
Weight upper limit	200
Weight lower limit	0

Table 4
Table of Comparisons

S_no	Type of Controller	Component	THD value (%)
1	Without using SAPF [38]	I_S (SourceCurrent)	18.42
2	PI based PV- SAPF	I_S (Source Current)	3.08
4	BBO tuned PI Based PV-SAPF	I_S (Source Current)	0.91
5	TLBO tuned ANN controller based PV-SAPF	I_S (SourceCurrent)	0.55

8.4 SAPF converter without DG integration scheme

The SAPF converter does not receive any supply from the PV panel. This means that this converter acts like only the FACT controller, which will inject the required reactive power into the load, and the load requires active power taken from the grid itself. From Figures 19, 20, and 21, we can clearly observe that the load required an active power of 5226 w and a reactive power of 2058 VAR. The reactive power was supplied only from the SAPF inverter, and the active power was supplied from the grid. Such that the SAPF converter without the DG integration mode acts as the FACT controller.

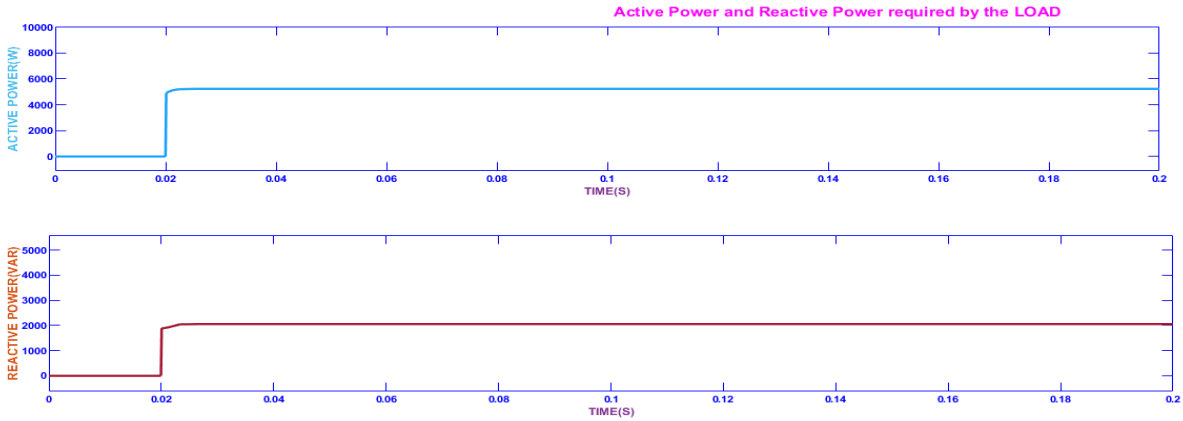

Fig. 19. Required Active power & Reactive power by non-linear load

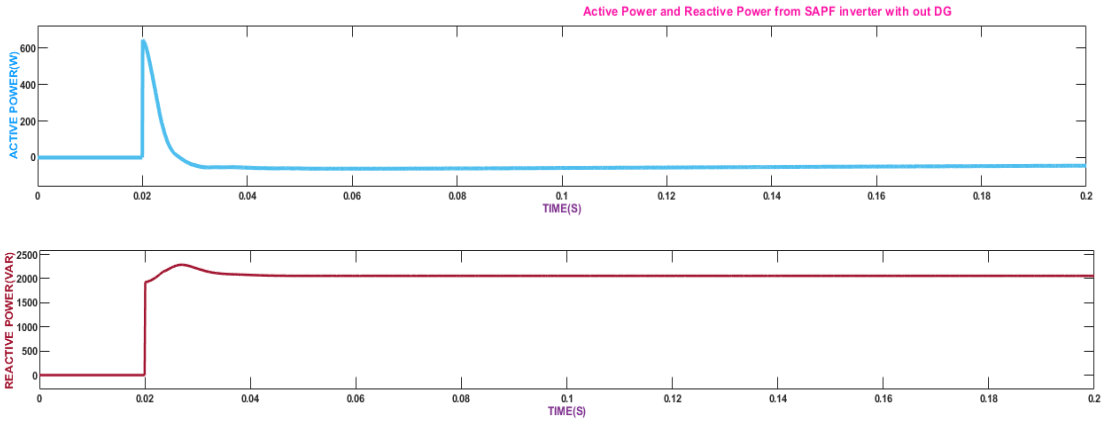

Fig. 20. Active power & Reactive power from SAPF inverter without DG

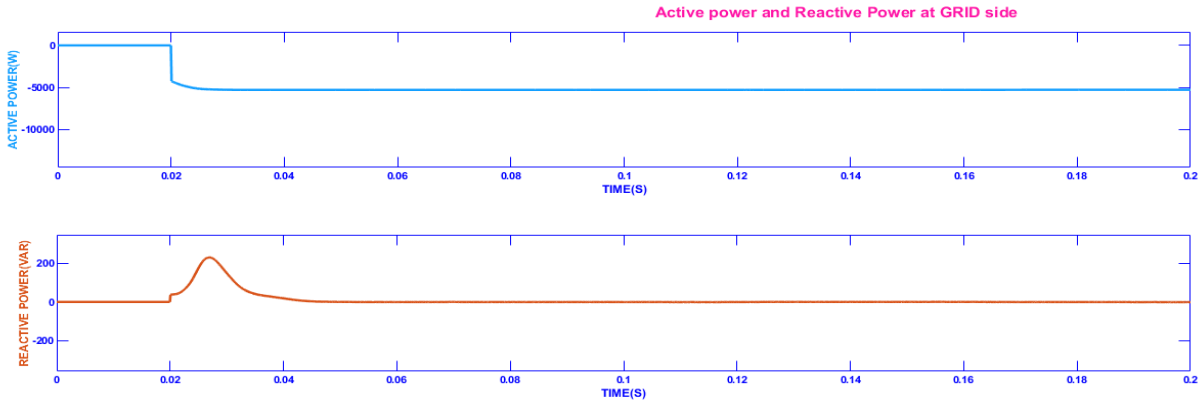

Fig. 21. Active power & Reactive power from the GRID

8.5 SAPF converter with DG integration scheme

The SAPF converter received a supply from the PV panel. This means that this converter acts like a DG converter as well as a FACT controller, which will inject the required reactive power into the load and active power. If the power required from the converter to the load is insufficient, the load will take the remaining required power from the grid. If there is excess power from the SAPF converter, it is sent to the GRID. From Figure 22, we can clearly observe that the load required an active power of 5226 w and a reactive power of 2058 VAR. Only the SAPF converter supplied the reactive power, and the same SAPF converter also supplied the necessary active power, as shown in Figure 23 and Figure 24.From that, the PV-SAPF converter actually has 25 KW of real power, but the load requires only 5226 W of real power, which is supplied from the PV-SAPF inverter, and the remaining 20 KW of real power is sent to GRID for future purposes. Such that the SAPF converter with DG integration mode acts as the FACT controller as well as the DG.

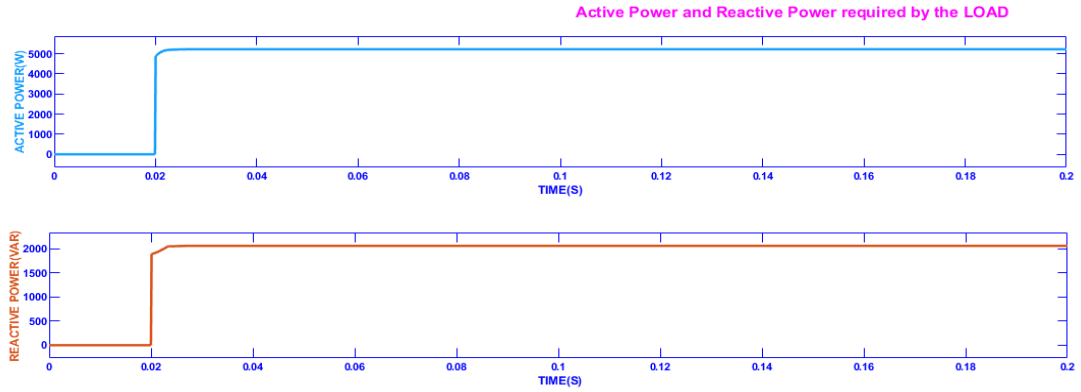

Fig. 22. Required Active power & Reactive power by non-linear load under DG integration

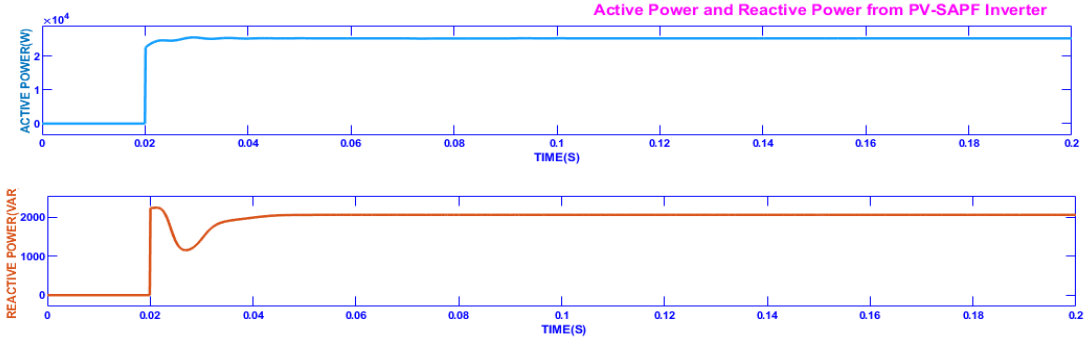

Fig. 23. Active power & Reactive power from PV integrated SAPF inverter

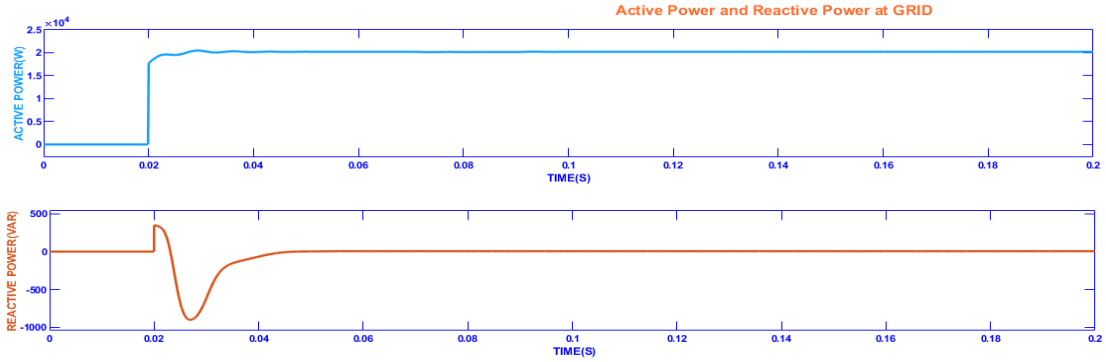

Fig. 24. Active power & Reactive power at the GRID side

9. Conclusions

The scope and complexity of power quality problems like harmonics and reactive power are constantly growing. Using strategies from artificial intelligence, it has been found that active filters can be made better at correcting reactive power and reducing harmonics. Total harmonic distortion can be reduced at the source end of the distribution network by implementing the TLBO-ANN control method proposed in this article.

The design of a photovoltaic (PV) integrated shunt active power filter is presented in this paper. It is made up of an artificial neural network (ANN) for DC-link control that was trained using teaching and learning-based optimization (TLBO). It works best when the voltage is right. To improve the power quality by reducing the total harmonic distortion (THD), this configuration was set up as follows: The software Matlab-Simulink simulates two different situations and then shows the results. With conventional PI controller-based PV-SAPF and BBO-tuned PI-based PV-SAPF, the THD remained at a minimum. The proposed TLBO-trained ANN-based PV-SAPF does a superior job of reducing the THD in the source current than the BBO-tuned PI-based PV-SAPF. The proposed BBO-trained PV-SAPF provides reactive power and also supplies active power when the load requires it (DG functionality).

In the near future, this proposed shunt active power filter will be implemented hardware-in-loop. ANNs, ANFIS controllers, and other optimization strategies can be used to make the PV-integrated SAPF respond better.

Author Contributions

The theoretical formalism, analytical estimations, and computational simulations were all created and executed by Venkata Anjani Kumar G. The original draft was written by Venkata Anjani Kumar G, and M. Damodar Reddy oversaw the entire project.

References

[1] Hassaine, L., E. Olias, J. Quintero, and M. Haddadi. "Digital power factor control and reactive power regulation for grid-connected photovoltaic inverter." *Renewable Energy* 34, no. 1 (2009): 315-321. https://doi.org/10.1016/j.renene.2008.03.016.

[2] Hamrouni, N., M. Jraidi, and A. Cherif. "New control strategy for 2-stage grid-connected photovoltaic power system." *Renewable Energy* 33, no. 10 (2008): 2212-2221. https://doi.org/10.1016/j.renene.2007.12.021.

[3] Villalva, Marcelo Gradella, Jonas Rafael Gazoli, and Ernesto Ruppert Filho. "Comprehensive approach to modeling and simulation of photovoltaic arrays." *IEEE Transactions on power electronics* 24, no. 5 (2009): 1198-1208. https://doi.org/10.1109/TPEL.2009.2013862.

[4] Langella, Roberto, Alfredo Testa, and Et Alii. "IEEE recommended practice and requirements for harmonic control in electric power systems." In *IEEE Recommended Practice*. IEEE, 2014. https://doi.org/10.1109/IEEESTD.2014.6826459.

[5] Sharma, Pooja, Siddhartha P. Duttagupta, and Vivek Agarwal. "A novel approach for maximum power tracking from curved thin-film solar photovoltaic arrays under changing environmental conditions." *IEEE Transactions on Industry Applications* 50, no. 6 (2014): 4142-4151. https://doi.org/10.1109/TIA.2014.2322136.

[6] Kazemzadeh, R., E. Najafi Aghdam, M. Fallah, and Y. Hashemi. "Performance scrutiny of two control schemes based on DSM and HB in active power filter." *Journal of Operation and Automation in Power Engineering* 2, no. 2 (2014): 103-112.

[7] Özkaya, Hasan. "Parallel active filter design, control, and implementation." Master's thesis, Middle East Technical University, 2007.

[8] Pachaivannan, Nammalvar, Ramkumar Subburam, Umadevi Ramkumar, and Meganathan Padmanaban. "Fuzzy tuned real and reactive power regulation in GC-VSI for PV systems." *International Journal of Electronics* 110, no. 3 (2023): 547-563.

[9] Chilakapati, Lenin Babu, and T. Gowri Manohar. "Control Strategies for Enhancing Power Quality with Unified Power Quality Conditioner in a Solar-PV Integrated Utility System." *Int. J. Exp. Res. Rev* 35 (2023): 01-15. https://doi.org/10.52756/ijerr.2023.v35spl.001.

[10] AttiyaSoliman, A. M., T. A. Kandil, M. A. Mehanna, and S. K. El-Sayed. "Mitigation of the Effect of HVDC System on Power System Quality at Distribution Level." *Department of Electrical Power and Machines, Faculty of Engineering, Al-Azhar University, Egypt,(IJEIT) Volume* 4 (2014).
[11] Soliman, A. M. A., S. K. El-Sayed, and M. A. Mehanna. "Assessment of Control Strategies for Conventional and Multi-functional Inverter Interfacing Power Grid with Renewable Energy Sources (RES)" *International Journal of Scientific & Engineering Research* 12, no. 4, 2017.
[12] Sabarimuthu, M., N. Senthilnathan, N. Priyadharshini, M. Arun Kumar, Nagarjuna Telagam, and S. Krithika Sree. "Comparison of current control methods for a three phase shunt active filter." In *2021 7th International Conference on Electrical Energy Systems (ICEES)*, pp. 32-37. IEEE, 2021. https://doi.org/10.1109/ICEES51510.2021.9383754
[13] Sao, Jitendra Kumar, Ramasamy Thaiyal Naayagi, Gayadhar Panda, Ram Dayal Patidar, and Sushree Diptimayee Swain. "SAPF Parameter Optimization with the Application of Taguchi SNR Method." *Electronics* 11, no. 3 (2022): 348. https://doi.org/10.3390/electronics11030348.
[14] Acharya, Devi Prasad, Subhashree Choudhury, and Niranjan Nayak. "Optimal Design of Shunt Active Power Filter for Power Quality Improvement and Reactive Power Management Using nm-Predator Prey Based Firefly Algorithm." *International Journal of Renewable Energy Research (IJRER)* 12, no. 1 (2022): 383-397.
[15] Babu, B. Mahesh, N. Uday Kumar, K. Santhosh Kumar, A. Amarendra, and B. Bindhu. "SAPF for Power Quality Improvement Based on PSODE Optimization Algorithm." *International Journal of Engineering and Advanced Technology (IJEAT)* 9, no. 3 (2020). https://doi.org/10.35940/ijeat.B2517.029320
[16] Avila, Victor Habermann, and Vicente Leite. "Control of grid-connected inverter output current: A practical review." In *2020 9th International Conference on Renewable Energy Research and Application (ICRERA)*, pp. 232-235. IEEE, 2020. https://doi.org/10.1109/ICRERA49962.2020.9242710
[17] Kennedy, James, and Russell Eberhart. "Particle swarm optimization." In *Proceedings of ICNN'95-international conference on neural networks*, vol. 4, pp. 1942-1948. IEEE, 1995. https://doi.org/10.1109/ICNN.1995.488968
[18] Bangia, Sakshi, P. R. Sharma, and Maneesha Garg. "Comparison of artificial intelligence techniques for the enhancement of power quality." In *2013 International Conference on Power, Energy and Control (ICPEC)*, pp. 537-541. IEEE, 2013. https://doi.org/10.1109/ICPEC.2013.6527715
[19] Vadi, Seyfettin, Fethi Batincan Gurbuz, Seref Sagiroglu, and Ramazan Bayindir. "Optimization of pi based buck-boost converter by particle swarm optimization algorithm." In *2021 9th International Conference on Smart Grid (icSmartGrid)*, pp. 295-301. IEEE, 2021. https://doi.org/10.1109/icSmartGrid52357.2021.9551229
[20] Oymak, Aysenur, and Mehmet Rida Tur. "A Short Review on the Optimization Methods Using for Distributed Generation Planning." *International Journal of smart grid-IJSMARTGRID* 6, no. 3 (2022): 54-64.
[21] Rao, Gundala Srinivasa, B. Srikanth Goud, and Ch Rami Reddy. "Power quality improvement using ASO technique." In *2021 9th International Conference on Smart Grid (icSmartGrid)*, pp. 238-242. IEEE, 2021. https://doi.org/10.1109/icSmartGrid52357.2021.9551226
[22] Karuppanan, P. "Design and Implementation of Shunt Active Power Line Conditioner using Novel Control Strategies." PhD diss., 2012.
[23] Mohapatra, Soumya Ranjan, and Pravat Kumar Ray. "A fixed switching frequency adaptive sliding mode controller for shunt active power filter system." In *TENCON 2014-2014 IEEE Region 10 Conference*, pp. 1-6. IEEE, 2014. https://doi.org/10.1109/TENCON.2014.7022318
[24] Tekwani, P. N., Ashwin Chandwani, Sagar Sankar, Neel Gandhi, and Siddharthsingh K. Chauhan. "Artificial neural network-based power quality compensator." *International Journal of Power Electronics* 11, no. 2 (2020): 256-282. https://doi.org/10.1504/IJPELEC.2020.105151
[25] Wilamowski, Bogdan M., and Hao Yu. "Improved computation for Levenberg–Marquardt training." *IEEE transactions on neural networks* 21, no. 6 (2010): 930-937. https://doi.org/10.1109/TNN.2010.2045657
[26] Kazemzadeh, R., E. Najafi Aghdam, M. Fallah, and Y. Hashemi. "Performance scrutiny of two control schemes based on DSM and HB in active power filter." *Journal of Operation and Automation in Power Engineering* 2, no. 2 (2014): 103-112.
[27] Farhan, Ahmad Fawwaz Irsyaad Ahmad, Nur Atiqah Mohamad Aziz, Hassan Mohamed, Bidattul Syirat Zainal, and Hazlina Junoh. "Investigation of the Thermal Performance of Water and Aluminum Oxide Nanofluid as a Coolant for Solar Panels." *Journal of Advanced Research in Fluid Mechanics and Thermal Sciences* 106, no. 2 (2023): 87-102.https://doi.org/10.37934/arfmts.106.2.87102
[28] Khudhur, Jawad, Abdulrazzak Akroot, and Ahmed Al-Samari. "Experimental Investigation of Direct Solar Photovoltaics that Drives Absorption Refrigeration System." *Journal of Advanced Research in Fluid Mechanics and Thermal Sciences* 106, no. 1 (2023): 116-135. https://doi.org/10.37934/arfmts.106.1.116135.
[29] Noui, Samir, Bekheïra Tabbache, El-Madjid Berkouk, and Mohamed Benbouzid. "A Pulse-Width Modulation Control Approach for the High-Voltage Gain Operation of a Z-Source Neutral-Point Clamped Inverters." *IETE Journal of Research* (2022): 1-20. https://doi.org/10.1080/03772063.2021.2021813

[30] Azad, Murari Lal, Soumya Das, Pradip Kumar Sadhu, Biplab Satpati, Anagh Gupta, and P. Arvind. "P&O algorithm based MPPT technique for solar PV system under different weather conditions." In *2017 International Conference on Circuit, Power and Computing Technologies (ICCPCT)*, pp. 1-5. IEEE, 2017. https://doi.org/10.1109/ICCPCT.2017.8074225.

[31] Salman, Salman, Xin Ai, and Zhouyang Wu. "Design of a P-&-O algorithm based MPPT charge controller for a stand-alone 200W PV system." *Protection and control of modern power systems* 3, no. 1 (2018): 1-8. https://doi.org/10.1186/s41601-018-0099-8

[32] Kumari, J. Surya, Dr Ch Sai Babu, and A. Kamalakar Babu. "Design and analysis of P&O and IP&O MPPT techniques for photovoltaic system." *International Journal of Modern Engineering Research* 2, no. 4 (2012): 2174-2180.

[33] Asadi, Yousef, Mohsen Eskandari, Milad Mansouri, Sajjad Chaharmahali, Mohammad H. Moradi, and Mohammad Sajjad Tahriri. "Adaptive Neural Network for a Stabilizing Shunt Active Power Filter in Distorted Weak Grids." *Applied Sciences* 12, no. 16 (2022): 8060. https://doi.org/10.3390/app12168060

[34] Rao, R. Venkata, Vimal J. Savsani, and D. P. Vakharia. "Teaching–learning-based optimization: a novel method for constrained mechanical design optimization problems." *Computer-aided design* 43, no. 3 (2011): 303-315. https://doi.org/10.1016/j.cad.2010.12.015

[35] Rao, R. Venkata, Vimal J. Savsani, and D. P. Vakharia. "Teaching–learning-based optimization: an optimization method for continuous non-linear large scale problems." *Information sciences* 183, no. 1 (2012): 1-15. https://doi.org/10.1016/j.ins.2011.08.006

[36] Venkata Anjani Kumar G and M. Damodar Reddy. ˝Fuzzy and PSO tuned PI controller based SAPF for Harmonic Mitigation." *International Journal of Electrical and Electronics Research*, *11*(1), (2023):119–125. https://doi.org/10.37391/IJEER.110116

[37] Venkata Anjani Kumar G. and M. Damodar Reddy, "PSO Trained Feed Forward Neural Network Based SAPF for Power Quality Enhancement in Distribution Networks," *International Journal of Electrical and Electronic Engineering & Telecommunications* 12, no. 4, (2023):279-287. https://doi.org/10.18178/ijeetc.12.4.279-287

[38] Reddy, M. Damodar. "Mitigation of Grid Current Harmonics by ABC-ANN based Shunt Active Power Filter." *Journal of Advanced Research in Applied Sciences and Engineering Technology* 33, no. 1 (2023): 285-298. https://doi.org/10.37934/araset.33.1.285298